Effect of Compatibilizer on Micromehanical Deformations and Morphology of Dispersion in PP/PDMS Blend

K. Prakashan, A. K. Gupta, S. N. Maiti

Centre for Polymer Science and Engineering, Indian Institute of Technology Delhi, New Delhi 110016, India

Received 18 August 2006; accepted 11 December 2006
DOI 10.1002/app.26510
Published online 16 May 2007 in Wiley InterScience (www.interscience.wiley.com).

ABSTRACT: Role of maleic anhydride grafted polypropylene (PP-*g*-MAH) in interface modification in polypropylene (PP)/poly(dimethylsiloxane) (PDMS) elastomer blend has been investigated in this article through its effects on morphology of dispersion, micromechanical deformations such as voiding, crazing, shear yielding, fibrillation, and tensile behavior. During tensile deformation, PP/PDMS blend without the compatibilizer showed debonding at the elastomer-matrix interface and it induced shear yielding and subsequently fibrillation in the matrix. The compatibilizer improved the interfacial adhesion between the PDMS domains and PP matrix, which prevented the debonding at elastomer-matrix interface and the resulting shear yielding, and fibrillation was absent and rather caused extensive crazing in the matrix. Addition of PP-*g*-MAH reduced the size of dispersed PDMS domains, and narrowed the domain size distribution, which is attributed as an effect of interfacial adhesion produced by PP-*g*-MAH. Stress–strain curve and fibrillation also show similar effect of the interfacial adhesion caused by the compatibilizer. All these observations consistently lead to conclude that PP-*g*-MAH acts as a good compatibilizer for PP/PDMS blend. © 2007 Wiley Periodicals, Inc. J Appl Polym Sci 105: 2858–2867, 2007

Key words: polypropylene; poly(dimethylsiloxane) elastomer; compatibilization; voids; shear yielding

INTRODUCTION

Isotactic polypropylene (PP) is an important thermoplastic widely studied owing to its varieties of applications ranging from household furniture to structural applications in automobiles. Elastomer modification is a long practiced method to improve the toughness of this polymer. This is particularly due to the ability of elastomer domains to initiate various energy absorbing micromechanical deformations in the PP matrix. These micromechanical deformations include crazing, shear yielding, voiding (internal cavitations of elastomer domains or debonding at the elastomer matrix interface), and dilatational shear yielding. The characteristics of these different micromechanical processes are described by Bucknall et al.[1,2] and Zebarjad et al.[3] The role of voiding as a toughening mechanism in elastomer-modified polymer matrix has been illustrated by many authors.[4–8] Voiding relieves the buildup of local hydrostatic tension around the rubber particles and the triaxial stress condition thus generated in the matrix is transformed to plane stress conditions, which give rise to shear yielding of the matrix. It is also reported that the voids can be concentrated in localized regions to form dilatational shear bands.[9,10] Depending on the interfacial adhesion and the elastomer properties, the voiding can occur inside the rubber particles (internal cavitations of elastomer) or at the interface (debonding).

In this article, we have studied tensile behavior and morphology of PP/PDMS blend in presence and absence of a compatibilizer, maleic anhydride grafted polypropylene (PP-*g*-MAH). The observed changes in the tensile behavior were correlated with the interfacial adhesion of the PDMS elastomer and the PP matrix. A correlation of the tensile behavior, morphology, and observations on voiding and other micromechanical deformation processes are presented and discussed for the effectiveness of compatibilizer. In addition, we also report some unique fibrillation behavior observed for the blend during tensile deformation, which also throws light on the interfacial adhesion in the blend.

EXPERIMENTAL

Materials

PP used in this study was a homopolymer, Repol H200MK, obtained from Reliance Industries, Mumbai (MFI 20 at 230°C/2.16 kg). Maleic anhydride grafted PP (PP-*g*-MAH), was a product (OPTIM-405) of Pluss Polymers, New Delhi (MFI 55 at 230°C/2.16 kg). The maleic anhydride content of PP-*g*-MAH determined by titration method was 0.22 wt %. The poly(dime-

Correspondence to: A. K. Gupta (akgncute@hotmail.com).

Journal of Applied Polymer Science, Vol. 105, 2858–2867 (2007)

TABLE I
Description and Composition of Blend Samples

Sample name	PP parts by weight	PDMS parts by weight	PP-*g*-MAH by weight	Volume fraction of PDMS
PP	100	0	0	0
PP/E5	100	5	0	0.048
PP/E10	100	10	0	0.092
PP/E20	100	20	0	0.169
PP/E30	100	30	0	0.235
PP/E20/C4	96	20	4	0.169
PP/E20/C6	94	20	6	0.169
PP/E20/C8	92	20	8	0.169

thylsiloxane) (PDMS) elastomer used was a noncommercial grade (Silpren V-SS), with no filler or additive, obtained from GE Bayer Silicones, Bangalore. The average molecular weight of the PDMS was determined by viscosity method and it was found to be 250,000. The viscosity measurements were carried out in toluene at 25°C and the ''*k*'' and ''*a*'' values, which are calibrated to weight average molecular weight were sourced from standard reference book.[11]

Blending and preparation of test specimens

Blending was carried out in a twin screw extruder made by Japan Steel Works (JSW J75E IV-P) with an $L/D = 36$ and $D = 30$ mm. The materials were predried in a vacuum oven at 70°C for 3 h before blending. The extrusion was performed at a screw rpm of 250, keeping temperature profile 140, 150, 190, 205, 205, 205, 215, 215, 225, and 230°C from feed zone to the die zone. The extruded strands were quenched in a water bath and granulated. The granules were then dried in a vacuum oven at 70°C for 2 h and injection molded using a Demag L&T injection molding machine (Model PFY 40). The barrel temperature profile of the injection molding was 190, 220, 225, and 230°C, while the mold was at room temperature. Description of the various samples, thus prepared, is given in Table I. The E and C letters in the sample name indicate the elastomer (PDMS) and the compatibilizer (PP-*g*-MAH), respectively, and the digits following them denote their proportion in ''parts by weight.''

Tensile testing

The tensile tests were performed at room temperature (32°C) using Zwick universal testing machine (model Z010) according to the ASTM D 638 Type 1 procedure. The gauge length was 65 mm and the test was conducted at two cross head speeds: 50 and 5 mm/min.

Morphology characterization

Morphology of cryogenically fractured blend specimens was investigated perpendicular to the flow direction by scanning electron microscope, Ziess EVO 50 SEM machine. The samples were etched in toluene for 2 days to dissolve out PDMS and then the dried fracture surfaces were sputter coated with silver prior to scanning. From the micrographs, domain sizes of the elastomer phase were quantified using Leica qwin image analyzing software. The domains of dispersed phase were assumed to be spherical and the diameter is measured as the shortest distance passing through the center. The domain size implies ''domain diameter'' in this article. Optical micrographs of the micro fibrillation of the tensile specimens during tensile fracture were obtained by Leica optical microscope.

RESULTS AND DISCUSSION

Morphology

The SEM micrographs of PP/PDMS blend with varying elastomer contents are shown in Figure 1(a–d). Variations of the size of the dispersed phase domains are apparent. Frequency distributions of domain sizes for the blends seen in these micrographs are presented in Figure 2(a–d). These micrographs show that PP/PDMS blend forms two phase morphology with PDMS domains dispersed in the PP matrix. The number–average domain size (D_n), the weight–average domain size (D_w), and the polydispersity index (PDI) have been evaluated using eqs. (1–3), similar to the expressions used in molecular weight averages:

$$D_n = \sum n_i D_i \Big/ \sum n_i \tag{1}$$

$$D_w = \sum n_i D_i^2 \Big/ \sum n_i D_i \tag{2}$$

$$\mathrm{PDI} = D_w/D_n \tag{3}$$

Values of average domain diameters, D_n and D_w, are shown in Table II. These values show an increase in domain size with increasing elastomer content.

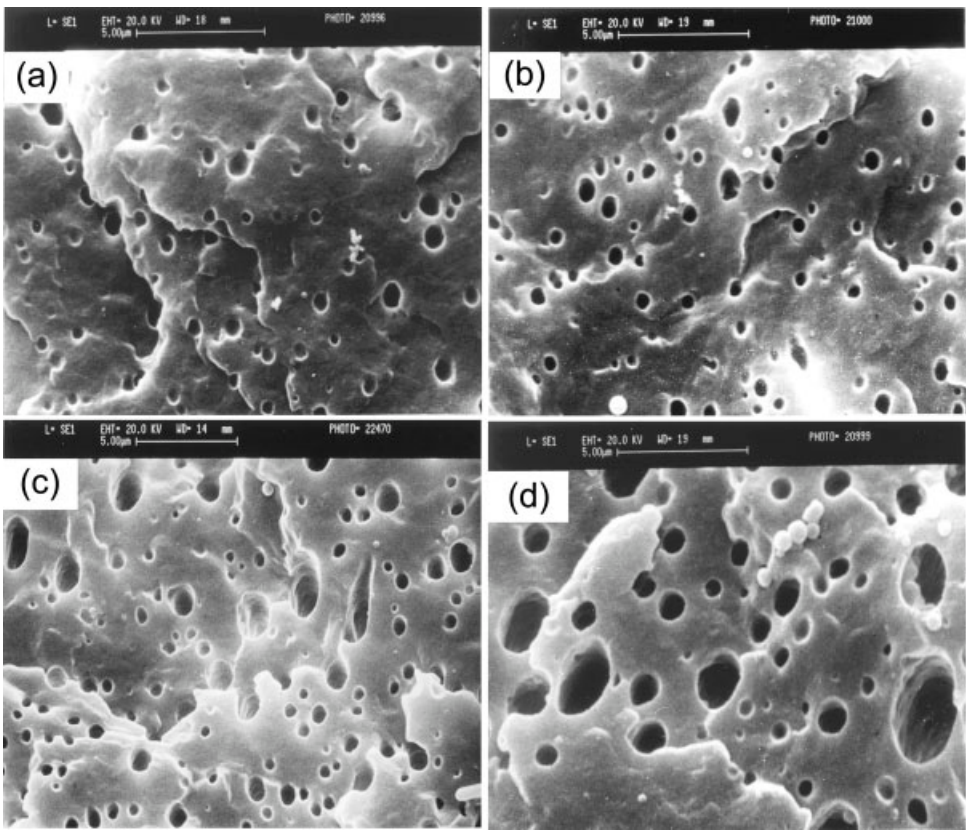

Figure 1 SEM micrographs of uncompatibilized PP/PDMS blend: (a) PP/E5, (b) PP/E10, (c) PP/E20, and (d) PP/E30.

This may be due to insufficient breakage of the dispersed phase droplets, or coalescence of already formed droplets. Coalescence may dominate at the higher volume fraction of dispersed phase. The domain size distribution, shown in Figure 2, indicates that at lower volume fraction of the dispersed phase, viz., 5 and 10 phr [Fig. 2(a,b)], the frequency of occurrence (in terms of number density) of small sized domains ($\sim$ 0.5 μm diameter) is higher than in the blend with higher volume fraction of dispersed phase, viz. 20 and 30 phr [Fig. 2(c,d)]. Moreover, the domain size distribution is very broad at the high volume fraction (viz. 30 phr) of the dispersed phase. This is also supported by the PDI values.

Effect of compatibilization on morphology

The PP/PDMS blend at a fixed composition (20 phr elastomer) was chosen for studying the compatibilization effect of PP-*g*-MAH. The compatibilizer content was varied in steps using 4, 6, and 8 wt % of the PP component of the blend, keeping the elastomer content constant at 20 phr in all samples. The SEM micrographs of fracture surfaces of uncompatibilized PP/PDMS blend (PP/E20) and the three blend samples at varying compatibilizer content are shown in Figure 3. Dispersed domains of the elastomer are clearly distinguishable in all these micrographs. Values of average domain diameters (D_n and D_w) and the PDI calculated using eqs. (1–3) are shown in Table III and the analysis of domain size distribution from these micrographs yields distribution patterns shown in Figure 4. These results show that as we go from 0 to 4% compatibilizer, the average domain size decreases [compare Fig. 3(a,b)], whereas in the case of 6 and 8 wt % compatibilizer content the decreasing trend of average domain size reverses with increasing compatibilizer content. The domain size distribution is narrow for the blend containing 4 wt % compatibilizer [Fig. 4(b)] compared to the corresponding uncompatibilized blend [Fig. 4(a)], but in samples with higher compatibilizer content domain size distribution is quite broad [Fig. 4(c,d)].

The domain size reduction and the narrowing of domain size distribution at 4 wt % compatibilizer when compared with the uncompatibilized blend is an indication of active role of the compatibilizer PP-*g*-MAH. The reduction in domain size is due to the reduction in interfacial tension between the PP and PDMS phase by the interaction of PP-*g*-MAH at the interface. PP-*g*-MAH has polar anhydride groups, which may form dipole–dipole interaction with the polar —Si—O—Si— bond in the PDMS chain while the nonpolar aliphatic components of the PP-*g*-MAH

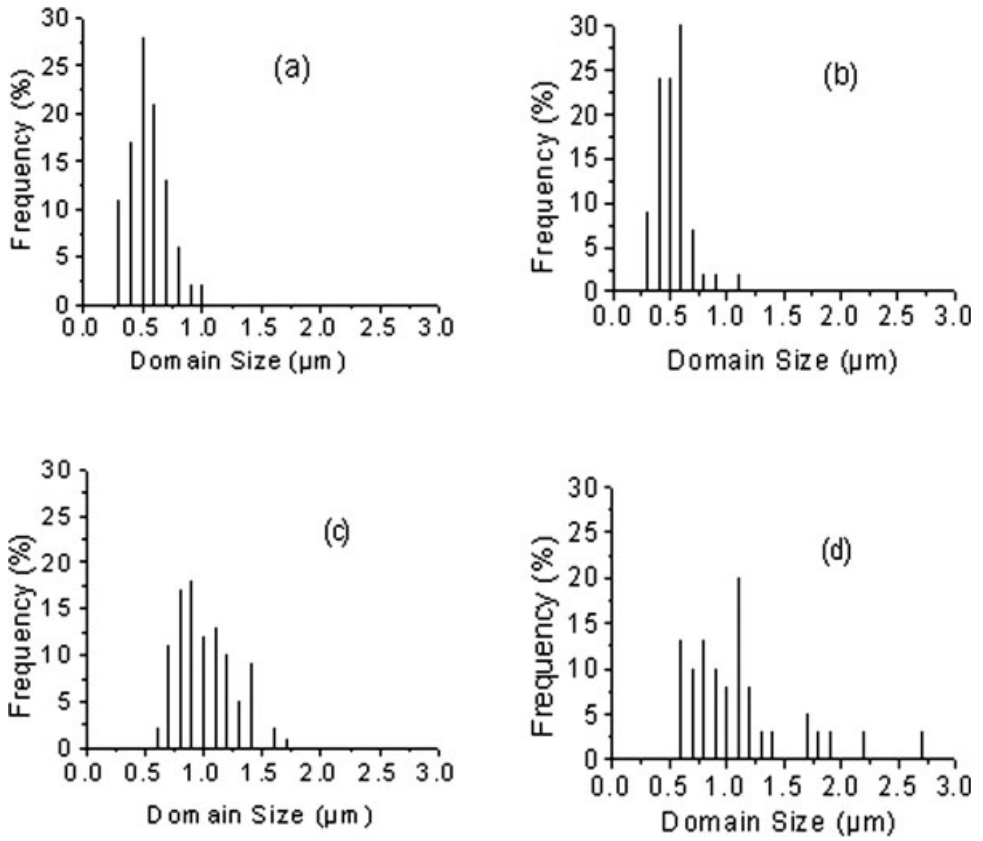

Figure 2 Domain size distribution of elastomer phase in uncompatibilized blend: (a) PP/E5, (b) PP/E10, (c) PP/E20, and (d) PP/E30.

can form physical entanglements with the PP matrix. At higher compatibilizer content (i.e., at 6 and 8 wt %), the reduction of domain size is less and the domain size distribution is broadened. This may be attributed to the effect of interfacial saturation of compatibilizer at a critical value of compatibilizer content above which the effect of compatibilizer on the domain size reduction levels off as has been observed in other systems.[12–15] Therefore, the higher effectiveness of compatibilizer in sample PP/E20/C4 may be due to the interfacial saturation occurring at this particular compatibilizer content (i.e., at 4 phr). In addition, the variation in viscosity ratio of the dispersed phase and the matrix caused by the incorporation of PP-*g*-MAH can also affect the domain size distribution. Because of the possibility of mixing of PP-*g*-MAH with PP the viscosity of the combined PP with PP-*g*-MAH phase will become lower and thus the viscosity ratio λ (defined as $\lambda = \lambda_{\text{dispersed}}/\lambda_{\text{matrix}}$) will increase. Thus, with increasing PP-*g*-MAH content, there will be an increase of the viscosity ratio, λ, which may be a reason for the observed less effectiveness of the compatibilizer in reducing domain sizes and its distribution at higher compatibilizer content.

The SEM micrographs of the fracture surfaces also show a higher surface roughness for the compatibilized blend (Fig. 3) when compared with the uncompatibilized blend (Fig. 1). The improved interfacial adhesion in case of the compatibilized blend renders the surrounding matrix to be tightly held by the elastomer domains during fracture, which causes the texture of the fracture surface to loose its flatness owing to three-dimensional distribution of dispersed domains.

Tensile properties

In absence of compatibilizer

Tensile stress–strain curves of PP and the uncompatibilized PP/PDMS blend at varying PDMS content are

TABLE II
Values of the Various Averages of Dispersed Phase Domain Size (Diameter), D_n and D_w, and the Polydispersity Index for PP/PDMS Blend

Sample name	D_n (μm)	D_w (μm)	PDI
PP/E5	0.54	0.59	1.08
PP/E10	0.54	0.59	1.08
PP/E20	1.00	1.06	1.06
PP/E30	1.06	1.28	1.21

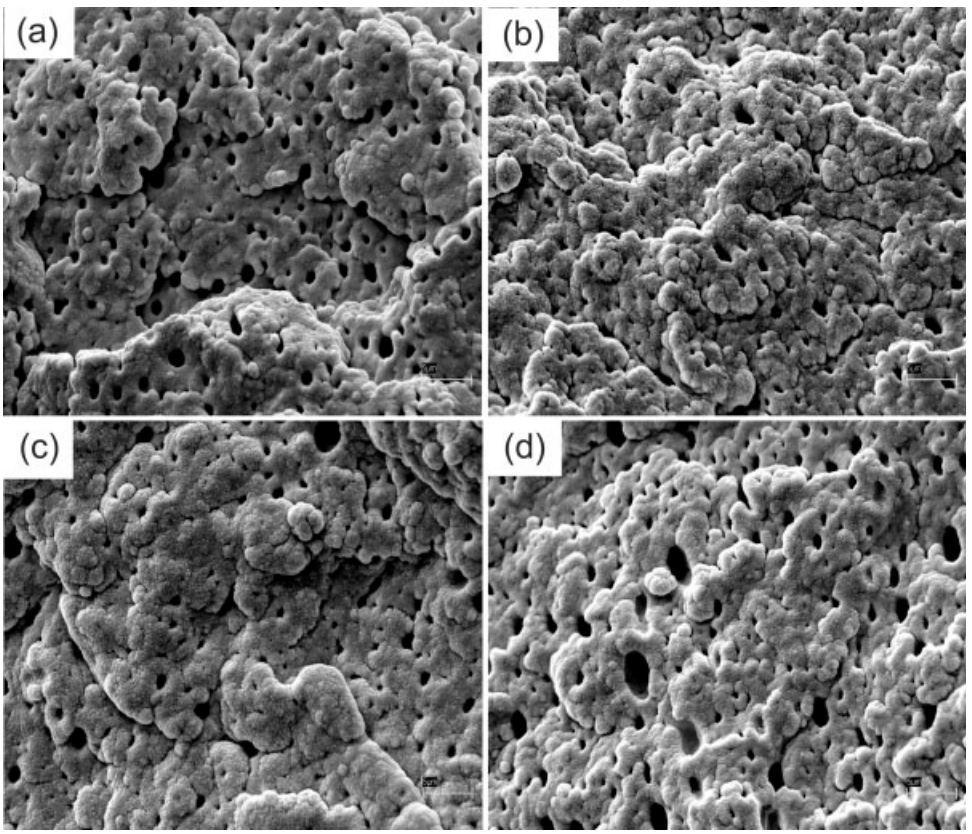

Figure 3 SEM micrographs of uncompatibilized blend: (a) PP/E20 and compatibilized blend: (b) PP/E20/C4, (c) PP/E20/C6, and (d) PP/E20/C8.

shown in Figure 5. The strain rate applied was 50 mm/min. The blends in all the compositions showed similar stress–strain curves, which were entirely different from that of PP. The PP specimen breaks immediately after the yield point at a strain of about 20%, whereas the blend samples showed an elongation up to 80–120% before fracture. Another noteworthy observation was the occurrence of fibrillation of specimens of the blends at high extension close to fracture. Such fibrillation was absent for PP and this will be discussed later.

It is further noteworthy that the stress–strain curves of the PP/PDMS blend comprise three distinct regions with different properties in each region. These three regions are marked A, B, and C in Figure 5 for the stress–strain curve of blend with 5 phr PDMS content (PP/E5).

The region A extending from origin up to the yield drop point of the stress–strain curve, which is similar to the stress–strain curve of PP up to its ultimate fracture. In this region, extensive stress whitening was observed for the blend specimens but no visible changes in the dimensions.

The region B consists of a nearly horizontal portion staring from the yield drop region to the beginning of the region C. Specimens showed a neck formation in the highly stress whitened zone of the specimen and the neck elongated during this part of the stress–strain curve. The neck formation and the subsequent cold drawing indicate the occurrence of shear yielding of the matrix. Such shear deformation and the cold drawing continued with very little variation of stress till the end of this region.

The region C represents a steep decrease in stress with the strain with some tendency of stabilization of stress in the middle. This region corresponds to the occurrence of fibrillation. Breaking of fibrils also occurs in this region and this manifests in the initial steep decrease of stress and this results in decrease of the cross section of the drawn specimen. There is a small horizontal portion in the middle of the region arising from an attempt by the highly oriented specimens to resist fracture. In the final stage, highly

TABLE III
Values of the Various Averages of Dispersed Phase Domain Size (Diameter), D_n and D_w, and the Polydispersity Index for Compatibilized PP/PDMS Blend

Sample name	D_n (μm)	D_w (μm)	PDI
PP/E20	1.00	1.06	1.06
PP/E20/C4	0.63	0.74	1.17
PP/E20/C6	0.80	0.92	1.15
PP/E20/C8	0.99	1.19	1.20

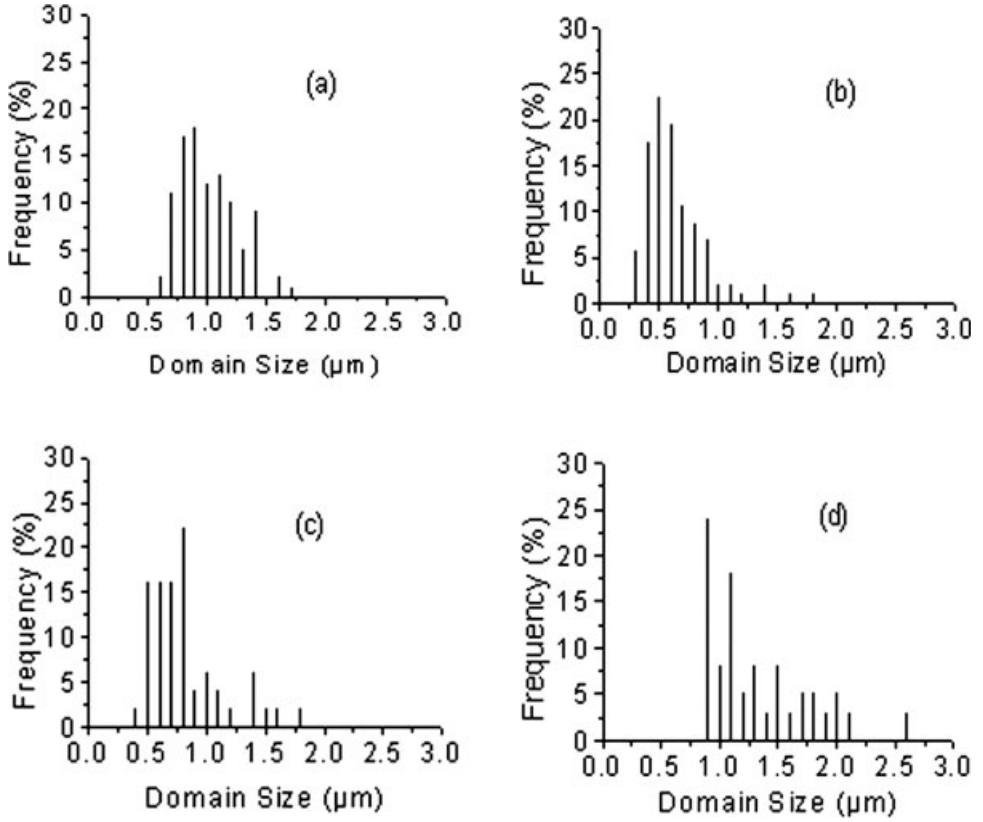

Figure 4 Domain size distribution of elastomer phase in uncompatibilized blend: (a) PP/E20 and in corresponding compatibilized blend: (b) PP/E20/C4, (c) PP/E20/C6, and (d) PP/E20/C8.

oriented fibrils of small cross section break at a very low value of stress or remain unbroken with a small bundle of fibrils connecting the two halves of the tensile specimen.

Photographs of the tensile specimens fractured at the rate of 50 mm/min are shown in Figure 6 for PP and selected samples of an uncompatibilized and compatibilized blend (PP/E20 and PP/E20/C4). From these photographs, it is clear that the specimen for PP and the compatibilized blend fractured without fibrillation, whereas the uncompatibilized blend fibrillated extensively. A small strip of the fibrils taken from the fibrillated PP/E20 specimen was examined through an optical microscope and the results are shown in Figure 7. The optical micrographs reveal a clear fibrillar structure in bundles as well as separated fibrils. The diameter of narrowest fiber, estimated from these micrographs, was around 5 μm.

This occurrence of fibrillation only in the blend without compatibilizer and its absence in the blend with compatibilizer suggests that the nonadhering nature of the PDMS gives rise to the separation of fibrils of the PP matrix in its highly sheared state during cold drawing. The lubricating effect of the PDMS domains may accelerate the cold drawing process and thus enhance fibrillation. At higher strain rate such as 50 mm/min, localized necking was observed in the specimen and a small cross section within the neck region may undergo high drawing and orientation, resulting in the PDMS domains getting oriented to form fibrils along the draw direction. Presence of PDMS fibrils is observed in the optical micrographs

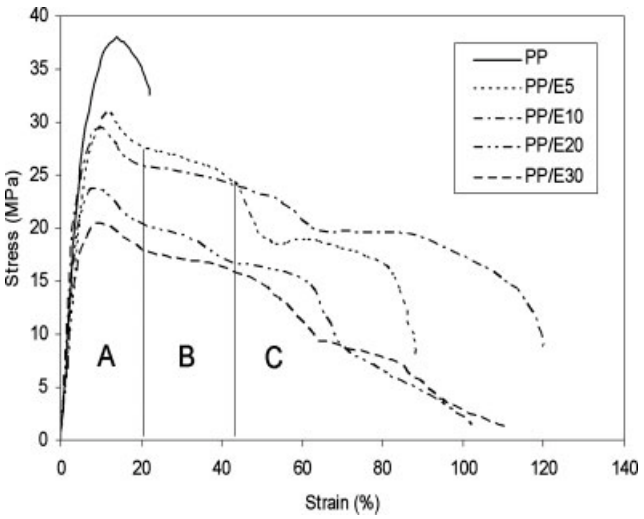

Figure 5 Stress–strain curves of PP and uncompatibilized PP/PDMS blend with varying elastomer content at a strain rate of 50 mm/min.

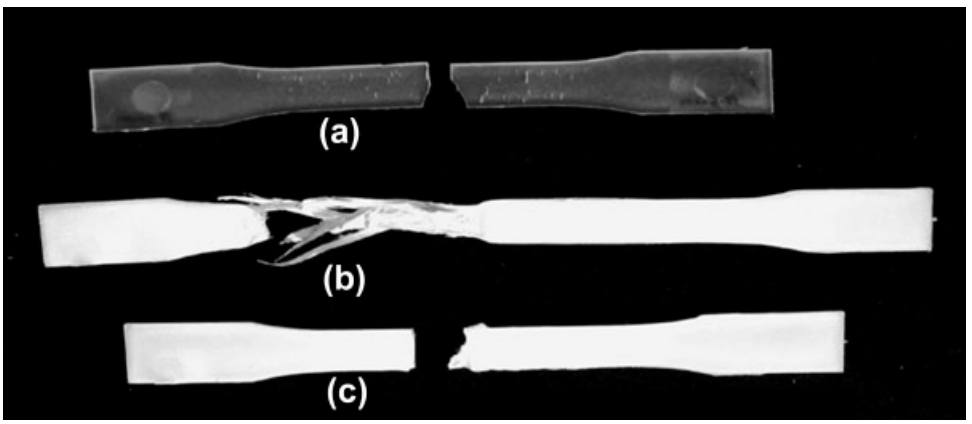

Figure 6 Photographs of the tensile specimens (a) PP, (b) uncompatibilized PP/E20 blend, and (c) compatibilized PP/E20/C4 blend fractured at a strain rate of 50 mm/min.

in Figure 7 through the nonstraight relaxed fibrils due to elastomeric nature of PDMS.

In presence of compatibilizer

The tensile stress–strain curves of the compatibilized PP/PDMS blend at fixed PDMS content (i.e., 20 phr) containing different proportion of the compatibilizer PP-*g*-MAH along with the curves of PP and the uncompatibilized blend having the same elastomer content (PP/E20) are shown in Figure 8. The characteristic features of the stress–strain curve are similar for all the compatibilizer contents but are distinctly different from that of uncompatibilized blend and that of PP. Yielding occurs in all the compatibilized blend samples at almost the same strain as that of uncompatibilized blend but the striking difference was the absence of necking. Other important differences in properties are the lower elongation at break (<40%) and higher stress at break for compatibilized

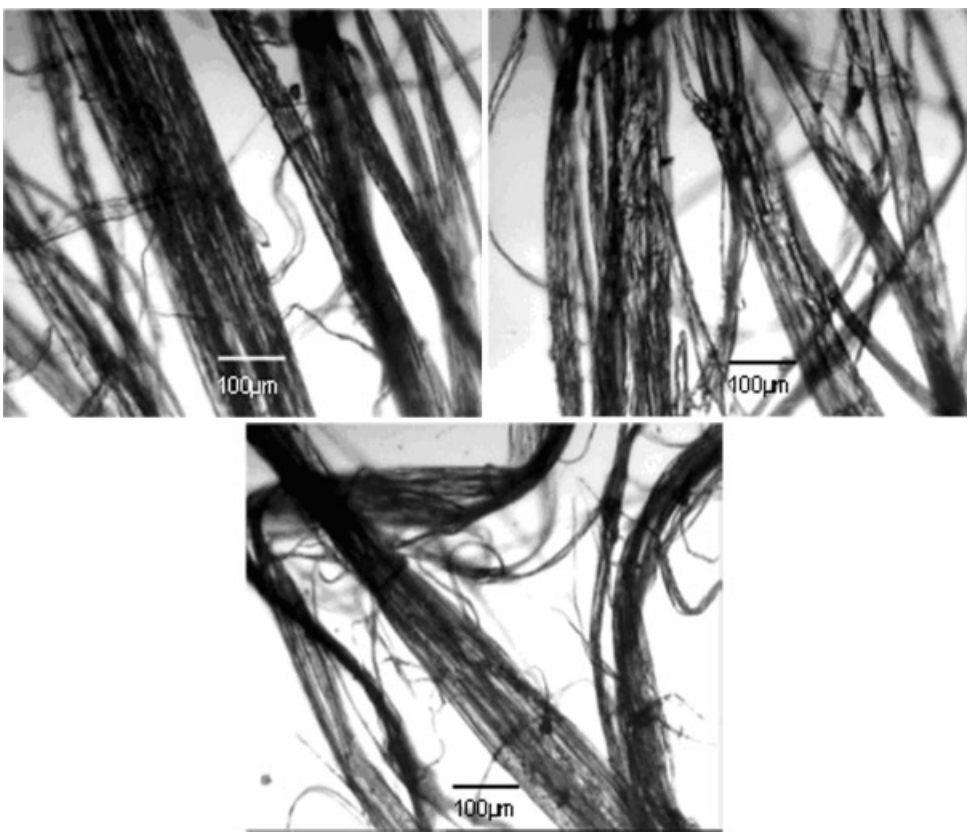

Figure 7 Optical micrographs of the microfibrils formed during tensile fracture of uncompatibilized PP/E20 blend.

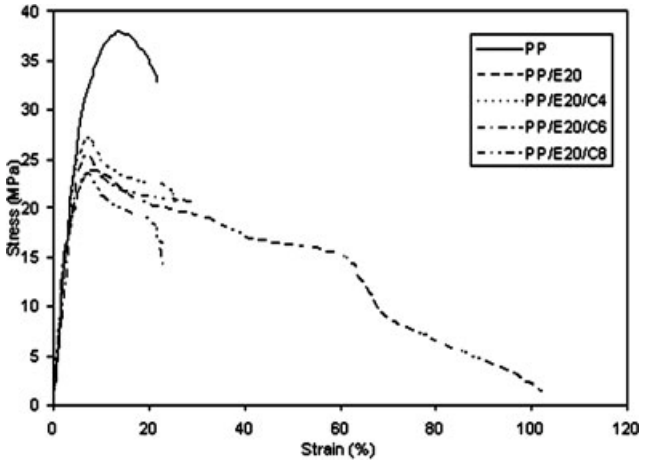

Figure 8 Stress–strain curves of compatibilized blend along with the corresponding uncompatibilized blend (PP/E20) and PP at a strain rate of 50 mm/min.

blend when compared with the uncompatibilized blend. Moreover, the fibrillation was absent in compatibilized blend [Fig. 6(c)]. The absence of necking and very low elongation at break in the blend with compatibilizer suggests that the interface adhesion prevents the shear yielding of the PP matrix and thus hampers cold drawing process for the compatibilized blend. Furthermore, we have observed the formation of macro crazes perpendicular to the draw direction, only in the case of compatibilized blend (Fig. 12), which is attributable to the strengthening of interfacial adhesion between PP and PDMS by the compatibilizer PP-*g*-MAH, as will be discussed later.

The tensile modulus (determined as slope of the initial portion of the stress–strain curve) and the yield strength (i.e., the stress at yield point) are higher in the case of compatibilized blend than the corresponding uncompatibilized blend in Figure 8. These higher values of modulus and the yield strength are due to the increased interfacial adhesion between PP and PDMS produced by the compatibilization effect of PP-*g*-MAH in PP/PDMS blend.

Strain rate dependence

Tensile stress–strain curves recorded at a lower test rate 5 mm/min of PP for compatibilized blend (PP/E20/C4) and corresponding uncompatibilized blend (PP/E20) are shown in Figure 9. The strain rate dependence on tensile deformation may be seen by comparing the corresponding stress–strain curves at the strain rate 50 mm/min shown in Figures 5 and 8. The stress–strain curve of PP and the compatibilized blends did not change much with the change in strain rate. But in the case of uncompatibilized blend, a very high elongation at break ($\sim$ 700%) was observed at the lower strain rate compared to its value ($\sim$ 120%) at the higher strain rate. The photographs of the tensile fractured specimens of PP, PP/E20, and PP/E20/C4 samples fractured at the lower strain rate (5 mm/min) are shown in Figure 10. Like the case of higher strain rate, fibrillation was absent for PP and the compatibilized blend, but the uncompatibilized blend showed fibrillation at the lower strain rate too.

Another notable difference in the behavior at lower and higher strain rates was the presence of multiple necking as compared with the single neck formation at high strain rate. At low strain rate, the specimen elongates almost uniformly throughout the gauge length and the breakage occurs not at the highly oriented middle portion but near to the grip of the specimen where there might be an inhomogeneity in the molecular orientation. Thus, it may be stated that at low strain rate the shear deformation occurs uniformly throughout the gauge length rather than occurring at a localized point, as in the case of high strain rate. This experiment also confirms that the shear yielding component in the deformation of PP and the compatibilized blend are too low to be affected by the change in strain rate.

Evidence of voiding

During tensile elongation stress whitening was observed only for the uncompatibilized blend starting at the yield. Neck formation preferentially occurred at a highly stress whitened zone of the specimen. Photographs of some tensile deformed specimens are shown in Figure 11 for the blend sample PP/E20: with no elongation (as a reference), and the same blend deformed up to the yield point and up to a certain extent of elongation beyond the yield point. These photographs clearly illustrate that uncompatibilized blend showed stress whitening at the yield

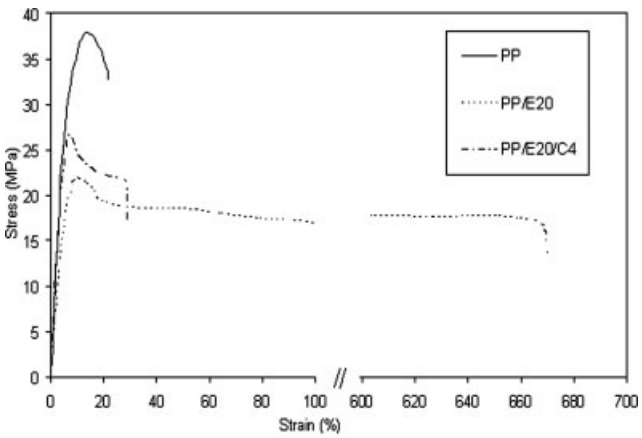

Figure 9 Stress–strain curves of PP, uncompatibilized PP/E20, and compatibilized PP/E20/C4 blend recorded at a strain rate of 5 mm/min.

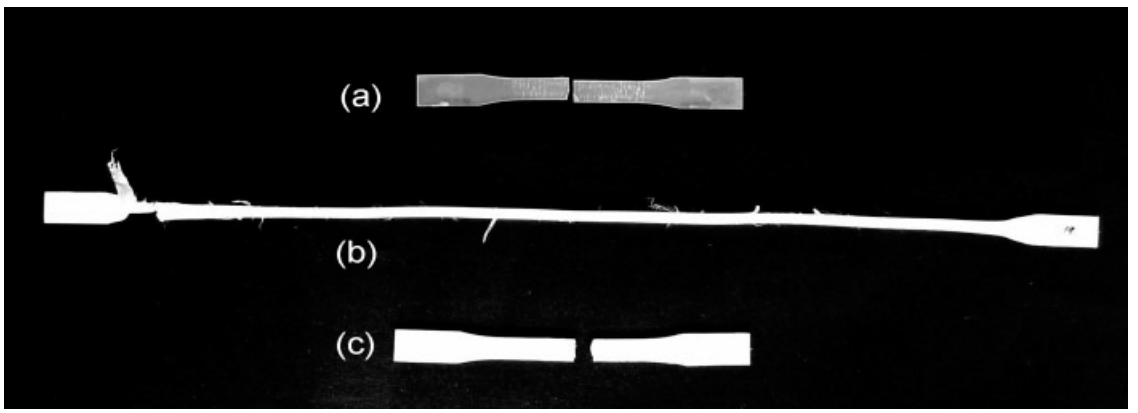

Figure 10 Photograph of the tensile fractured specimens of (a) PP, (b) uncompatibilized PP/E20, and (c) compatibilized PP/E20/C4 specimens at a test speed of 5 mm/min.

point and after the neck formation on each side of the neck [Fig. 11(b,c)]. Also included in Figure 11 is the photograph of a specimen of compatibilized blend PP/E20/C4 fractured during the test, showing no stress whitening, instead a large number of macro crazes appeared perpendicular to the draw direction of the specimen. These macro crazes are clearly visible in the close-up of Figure 11(d) shown in Figure 12.

It is believed that the stress whitening is due to formation of voids in the specimen. In elastomer-modified plastics, the formation of voids may be viewed as either by debonding at the elastomer matrix interface or by the internal cavitaion of the elastomer. In this case of PP/PDMS blend, the presence of stress whitening for uncompatibilized blend and the absence of the same for the compatibilized blend rules out the occurrence of voiding by internal cavitaion of elastomer. If the voiding was by internal cavitaion of elastomer, both the compatibilized and the uncompatibilized blends would have shown the stress whitening. Therefore, the present results lead us to believe that the main cause of voiding in the studied blend was the debonding at the elastomer matrix interface and the improved interfacial adhesion in case of the compatibilized blend prevented the debonding.

In the case of uncompatibilized blend, the observed necking and cold drawing is an evidence of shear yielding of the matrix. This seems to suggest that voiding initiated the shear yielding of PP matrix in PP/PDMS blend. Voiding relieves the buildup of local hydrostatic tension around the rubber domains

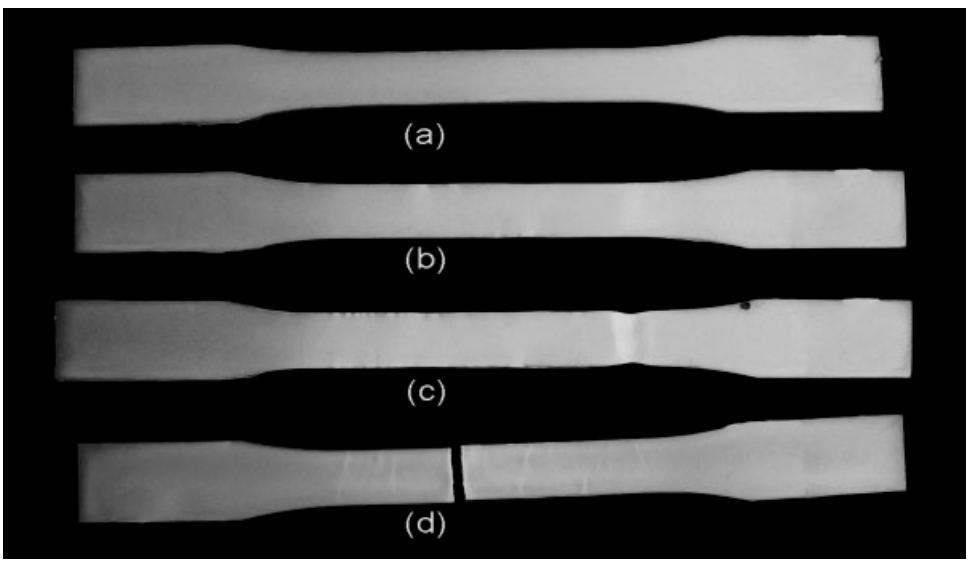

Figure 11 Photographs of the tensile specimens of (a) PP/E20 with no elongation, (b) PP/E20 elongated up to yield point, (c) PP/E20 elongated some distance beyond yield point, and (d) compatibilized PP/E0/C4 elongated up to fracture.

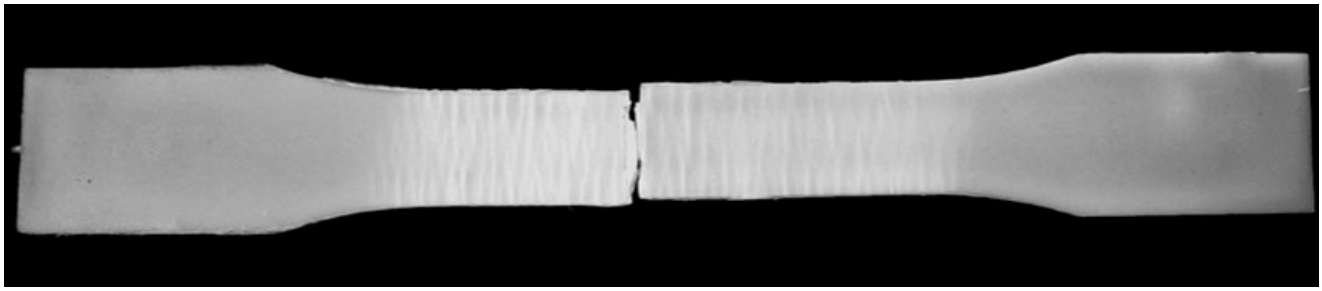

Figure 12 Macro crazes observed on the tensile fractured specimen of compatibilized PP/E20/C4 blend.

and the triaxial stress changes in to plane stress, which favors the shear yielding of the matrix. In case of the compatibilized blend, the improved interfacial adhesion not only prevented the debonding and subsequent shear yielding but also induced extensive crazing in the PP matrix.

CONCLUSIONS

The interfacial adhesion between the PDMS domains and PP matrix was found to be very weak and it caused debonding at the elastomer-matrix interface. This debonding initiated shear yielding and subsequently fibrillation in the PP/PDMS blend.

PP-*g*-MAH was found to be acting as a good compatibilizer for PP/PDMS blend. The compatibilizer caused improved interfacial adhesion between the PDMS domains and the PP matrix and in turn prevented the debonding of elastomer domains during deformation. Because of the absence of debonding shear yielding, the subsequent fibrillation was absent for compatibilized blend. The improved interfacial adhesion rather caused extensive crazing in the matrix.

The PP-*g*-MAH caused the reduction in size of the dispersed PDMS domains and narrowed the domain size distribution in compatibilized blend. It also improved the tensile properties and significantly altered the stress–strain behavior in compatibilized blend.

References

1. Bucknall, C. B. Toughened Plastics; Applied Science: London, 1977.
2. Lazzeri, A.; Bucknall, C. B. Polymer 1995, 36, 2895.
3. Zebarjad, S. M.; Bagheri, R.; Lazzeri, A.; Serajzadeh, S. Mater Des 2004, 25, 247.
4. Bucknall, C. B. Adv Polym Sci 1978, 27, 121.
5. Donald, A. M.; Kramer, E. J. J Mater Sci 1982, 17, 1765.
6. Yee, A. F.; Pearson, R. A. J Mater Sci 1986, 21, 2462.
7. Ramsteiner, F.; Heckmann, W. Polym Commun 1985, 26, 199.
8. Borggreve, R. J. M.; Gaymans, R. J.; Eichenwald, H. M. Polymer 1989, 30, 78.
9. Lazzeri, A.; Bucknall, C. B. J Mater Sci 1993, 28, 6799.
10. Lazzeri, A.; Bucknall, C. B. Polymer 1995, 36, 2895.
11. Bandrup, J.; Immergut, E. H. Polymer Handbook; Wiley: New York, 1975.
12. Fayt, R.; Jerome, R.; Teyssie, Ph. Polym Eng Sci 1987, 27, 328.
13. Willis, J. M.; Favis, B. D. Polym Eng Sci 1990, 30, 1073.
14. Cinaga, P.; Favis, B. D.; Jerome, R. J Polym Sci Part B: Polym Phys 1996, 34, 1691.
15. Kim, S. J. K.; Kim, S.; Park, C. E. Polymer 1997, 38, 2155.